Reconstruction of Current Distribution and Termination Impedances of PCB-Traces by Magnetic Near-Field Data and Transmission-Line Theory

Robert Nowak, Stephan Frei
TU Dortmund University
Dortmund, Germany
robert.nowak@tu-dortmund.de

***Abstract*—Various publications have shown methods to reconstruct the current distribution of a wire system, e.g. of a PCB, by the usage of near-field data. Especially, if there is knowledge about the potential current paths, these methods achieve satisfactory results. This publication presents a novel approach to improve the quality of the reconstruction by application of the transmission-line theory. Additionally, also the termination impedances of a PCB trace can be determined by the approach presented in this work. For demonstration, several PCB-like structures are investigated with the introduced methods. The results are discussed and compared to other methods.**

Keywords—current distribution; current reconstruction; near-field data; near-field scan; transmission-line theory; EMI analysis; impedance determination

I. Introduction

Near-field scans are more and more commonly used analysis methods for EMI investigations. Near-field data provides some advantages over antenna measurements. Calculation of the far-field of a PCB is possible by knowing the near-field distribution [1], [2]. Thus, near-field data can predict the result of an antenna measurement (see Fig. 1). Furthermore, from the near-field data, the interference sources might be identified by a search for high field strengths. In some cases, high local field strengths can be misleading, when no radiating structure is available. Due to this reason it can be advantageous to find the interference sources by the reconstruction of the current distribution in a PCB [3]. With knowledge of the possible current paths and current distribution along the paths critical structures can be identified and the estimation of the far-field is possible (see Fig. 1).

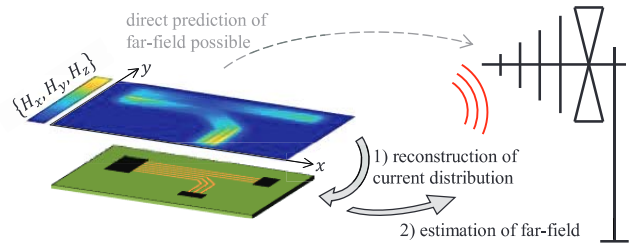

Fig. 1. Possible evaluations based on near-field data.

This paper presents the improvement of an existing method to reconstruct the current distribution. Starting point is the multi-dipole-model of a trace system from a PCB. By creating an inverse problem between the dipole currents of the multi-dipole-model and its near-field distribution, the current distribution can be determined. This method is described in [3] and summarized in II. A new approach to integrate the transmission-line theory in the inverse problem is presented in III. In addition, based on the transmission-line theory, two methods are derived to determine the termination impedances of the investigated wire system. Then, the presented methods are applied to simulation data. First, the current reconstruction of a PCB like structure is compared to simulation data in IV. Afterward, the methods for determining the termination impedance are used for examples in V. In VI, one of these methods is applied to measurement data. Finally, the results are summarized and an outlook on our further work is presented.

For all approaches in this paper, the amplitude and phase of the magnetic near field are assumed to be known. In addition, the position and propagation characteristics of the current paths must be known.

II. Basic Method for Finding the Current Distribution

Firstly, the magnetic field of an arbitrary oriented current is modelled by three orthogonal electric dipoles. These three dipoles are summed up to a dipole-triple. The current of the j-th dipole-triple at the position $\mathbf{x}_{\mathrm{D,j}}$ induces $\mathbf{H}_{\mathrm{i}}$ at the observation point $\mathbf{x}_{\mathrm{O,i}}$:

$$\underbrace{\begin{bmatrix} H_{\mathrm{x}}(\mathbf{x}_{\mathrm{O,i}}) \\ H_{\mathrm{y}}(\mathbf{x}_{\mathrm{O,i}}) \\ H_{\mathrm{z}}(\mathbf{x}_{\mathrm{O,i}}) \end{bmatrix}}_{\mathbf{H}_{\mathrm{i}}} = \boldsymbol{\Psi}(\mathbf{x}_{\mathrm{O,i}}, \mathbf{x}_{\mathrm{D,j}}) \cdot \underbrace{\begin{bmatrix} \tilde{I}_{\mathrm{x,j}} \\ \tilde{I}_{\mathrm{y,j}} \\ \tilde{I}_{\mathrm{z,j}} \end{bmatrix}}_{=\tilde{\mathbf{I}}_{\mathrm{j}}} \tag{1}$$

Here, the current is described by the dipole moments $\tilde{I}_{\mathrm{x,j}}$, $\tilde{I}_{\mathrm{y,j}}$ and $\tilde{I}_{\mathrm{z,j}}$. The matrix $\boldsymbol{\Psi}(\mathbf{x}_{\mathrm{O,i}}, \mathbf{x}_{\mathrm{D,j}})$ is based on the typical field description of an elemental dipole like in [4]. In the multi-dipole-model, there is a defined number of dipole-triples used to represent all current paths. Therefore, the n dipole-triples are positioned at the lanes of the investigated PCB and the superposition represents the induced magnetic field $\mathbf{H}$ at m points:

$$\underbrace{\begin{bmatrix}\mathbf{H}_1\\ \mathbf{H}_2\\ \vdots\\ \mathbf{H}_\mathrm{m}\end{bmatrix}}_{=\mathbf{H}} = \underbrace{\begin{bmatrix}\boldsymbol{\Psi}(\mathbf{x}_{\mathrm{O},1},\mathbf{x}_{\mathrm{D},1}) & \cdots & \boldsymbol{\Psi}(\mathbf{x}_{\mathrm{O},1},\mathbf{x}_{\mathrm{D,n}})\\ \boldsymbol{\Psi}(\mathbf{x}_{\mathrm{O},2},\mathbf{x}_{\mathrm{D},1}) & \cdots & \boldsymbol{\Psi}(\mathbf{x}_{\mathrm{O},2},\mathbf{x}_{\mathrm{D,n}})\\ \vdots & \ddots & \vdots\\ \boldsymbol{\Psi}(\mathbf{x}_{\mathrm{O,m}},\mathbf{x}_{\mathrm{D},1}) & \cdots & \boldsymbol{\Psi}(\mathbf{x}_{\mathrm{O,m}},\mathbf{x}_{\mathrm{D,n}})\end{bmatrix}}_{=\boldsymbol{\Psi}} \cdot \underbrace{\begin{bmatrix}\tilde{\mathbf{I}}_1\\ \vdots\\ \tilde{\mathbf{I}}_\mathrm{n}\end{bmatrix}}_{=\tilde{\mathbf{I}}} \tag{2}$$

The matrix $\boldsymbol{\Psi}$ represents the effect of all dipole moments $\tilde{\mathbf{I}}$ on the magnetic field. If there are more (or equal) observation points m than dipole-triples n, (2) can be interpreted as an inverse problem. The Tikhonov regularization is a recommended approach to solve this problem [5], [6].

It is possible to interpret the dipole moments of a dipole-triple with its spatial expansion and total current flow. For this purpose, the straight lines of the investigated wire system must be defined by starting point, endpoint and number of used dipole-triples. For the i-th line these features are named $\mathbf{p}_{\mathrm{S,i}}$, $\mathbf{p}_{\mathrm{E,i}}$ and N_i. In Fig. 2, this exemplary line and the j-th dipole-triple, which is part of the line, are shown. Starting point and endpoint define the direction

$$\mathbf{e}_\mathrm{j} = \frac{1}{\left|\mathbf{p}_{\mathrm{E,i}} - \mathbf{p}_{\mathrm{S,i}}\right|}\left(\mathbf{p}_{\mathrm{E,i}} - \mathbf{p}_{\mathrm{S,i}}\right) \tag{3}$$

of the current flow I_j. Also, these points specify the total length

$$l_\mathrm{j} = \frac{1}{N_\mathrm{i}}\left|\mathbf{p}_{\mathrm{E,i}} - \mathbf{p}_{\mathrm{S,i}}\right| \tag{4}$$

of the j-th dipole-triple and each other dipole-triple in the i-th line. The combination of direction $\mathbf{e}_\mathrm{j}$, total current I_j and total length l_j represents the total dipole moment as

$$\tilde{\mathbf{I}}_\mathrm{j} = I_\mathrm{j} l_\mathrm{j} \cdot \mathbf{e}_\mathrm{j}\,. \tag{5}$$

This allows the representation of (2) as

$$\mathbf{H} = \boldsymbol{\Psi} \cdot \underbrace{\underbrace{\begin{bmatrix} l_1\cdot\mathbf{e}_1 & & \mathbf{0}\\ & l_2\cdot\mathbf{e}_2 & \\ & & \ddots\\ \mathbf{0} & & l_\mathrm{n}\cdot\mathbf{e}_\mathrm{n}\end{bmatrix}}_{=\mathbf{D}_\mathrm{l}} \cdot \begin{bmatrix}I_1\\ I_2\\ \vdots\\ I_\mathrm{n}\end{bmatrix}}_{=\tilde{\mathbf{I}}}. \tag{6}$$

In this step, the current is separated from the dipole moments. Thus, the inverse problem between the observed magnetic field and the inducing currents can be described by (6).

III. Novel Approach

A. Involving the Transmission-line Theory in the Inverse Problem and Determining the Line Termination Impedance

The definition of the inverse problem in (2) and (6) leads to a solution, which implies the current of every dipole. Therefore, it is possible, e.g. due to measurement noise, that the current distribution does not follow physical rules. In order to increase accuracy, in [7] an approach is described to link the phase of neighboring dipole currents. Different to this approach, this section shows an elementary modification of the inverse problem considering the transmission-line theory.

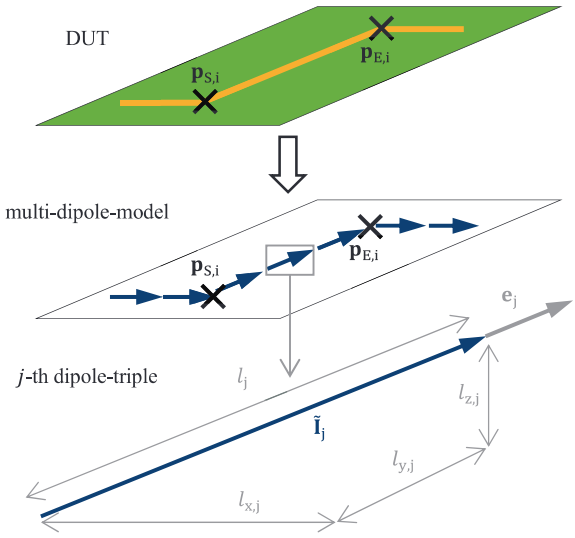

Fig. 2. Illustration of the j-th dipole-triple in a multi-dipole-model.

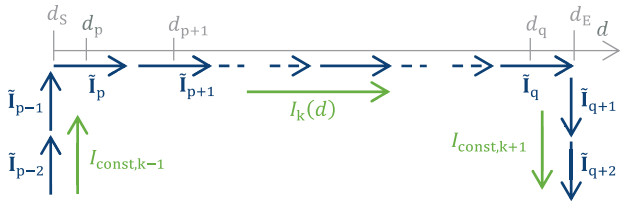

Fig. 3. Exemplary structure represented by dipoles.

The transmission-line theory generally describes current distribution on lines [4]. Therefore, the distribution of the k-th line can be formulated as superposition of an incident current wave $I_{\mathrm{i,k}}$ and a reflected current wave $I_{\mathrm{r,k}}$:

$$I(d) = I_{\mathrm{i,k}}\mathrm{e}^{-\gamma_\mathrm{k} d} - I_{\mathrm{r,k}}\mathrm{e}^{\gamma_\mathrm{k} d} \tag{7}$$

The propagation constant is given with γ_k, d is a an arbitrary position on the line. With knowledge of the propagation constant and the dipole positions, the currents of all dipole-triples representing a straight line can be substituted by only one incident wave and one reflected wave. In Fig. 3, an exemplary case is shown. The dipole-triples $\tilde{\mathbf{I}}_\mathrm{p}, \tilde{\mathbf{I}}_{\mathrm{p+1}}, \ldots, \tilde{\mathbf{I}}_\mathrm{q}$ carry the currents $I_\mathrm{p}, I_{\mathrm{p+1}}, \ldots, I_\mathrm{q}$ at the positions $d_\mathrm{p}, d_{\mathrm{p+1}}, \ldots, d_\mathrm{q}$. Considering (7), these currents are described by

$$\begin{bmatrix} e^{-\gamma_\mathrm{k} d_\mathrm{p}} & -e^{\gamma_\mathrm{k} d_\mathrm{p}}\\ e^{-\gamma_\mathrm{k} d_{\mathrm{p+1}}} & -e^{\gamma_\mathrm{k} d_{\mathrm{p+1}}}\\ \vdots & \vdots\\ e^{-\gamma_\mathrm{k} d_\mathrm{q}} & -e^{\gamma_\mathrm{k} d_\mathrm{q}}\end{bmatrix} \cdot \begin{bmatrix} I_{\mathrm{i,k}}\\ I_{\mathrm{r,k}}\end{bmatrix} = \begin{bmatrix} I_\mathrm{p}\\ I_{\mathrm{p+1}}\\ \vdots\\ I_\mathrm{q}\end{bmatrix} = \begin{bmatrix} I(d_\mathrm{p})\\ I(d_{\mathrm{p+1}})\\ \vdots\\ I(d_\mathrm{q})\end{bmatrix}. \tag{8}$$

The modelling of short line structures is also possible with a similar approach. If a constant value sufficiently approaches the current distribution, the presentation

$$\begin{bmatrix}1\\1\end{bmatrix} \cdot \left[I_{\mathrm{const,k-1}}\right] = \begin{bmatrix} I_{\mathrm{p-2}}\\ I_{\mathrm{p-1}}\end{bmatrix} \tag{9}$$

is possible for the dipole currents. So, all shown dipole currents in Fig. 3 are defined by four values:

$$\underbrace{\begin{bmatrix} 1 & & & \\ 1 & & & \\ & e^{-\gamma_k d_p} & -e^{\gamma_k d_p} & \\ & e^{-\gamma_k d_{p+1}} & -e^{\gamma_k d_{p+1}} & \\ & \vdots & \vdots & \\ & e^{-\gamma_k d_q} & -e^{\gamma_k d_q} & \\ & & & 1 \\ & & & 1 \end{bmatrix}}_{=\mathbf{K}_{sub}} \cdot \begin{bmatrix} I_{const,k-1} \\ I_{i,k} \\ I_{r,k} \\ I_{const,k+1} \end{bmatrix} = \begin{bmatrix} I_{p-2} \\ I_{p-1} \\ I_p \\ I_{p+1} \\ \vdots \\ I_q \\ I_{q+1} \\ I_{q+2} \end{bmatrix} \tag{10}$$

The consideration of Kirchhoff's current law allows an additional reduction of the relevant values. If there are not any other current paths, the currents $I_{const,k-1}$ and $I_{const,k+1}$ on the short lines are nearly equal to the currents at the near end and far end of the k-th line. Thus, the incident and reflected current waves are enough to represent all four values in (10):

$$\begin{bmatrix} I_{const,k-1} \\ I_{i,k} \\ I_{r,k} \\ I_{const,k+1} \end{bmatrix} = \underbrace{\begin{bmatrix} e^{-\gamma_k d_S} & -e^{\gamma_k d_S} \\ 1 & 0 \\ 0 & 1 \\ e^{-\gamma_k d_E} & -e^{\gamma_k d_E} \end{bmatrix}}_{=\mathbf{K}_{CL}} \cdot \begin{bmatrix} I_{i,k} \\ I_{r,k} \end{bmatrix} \tag{11}$$

Therefore, the inverse problem to determine the currents of the exemplary structure in Fig. 3 by using near field data is

$$\mathbf{H} = \mathbf{\Psi} \cdot \mathbf{D}_l \cdot \mathbf{K}_{sub} \cdot \mathbf{K}_{CL} \cdot \begin{bmatrix} I_{i,k} \\ I_{r,k} \end{bmatrix}. \tag{12}$$

Considering Kirchhoff's current law is also possible for junctions of two or more current paths, which current distributions are described with incident and reflected waves. If, for example, section k ends at the beginning of section $k+1$, the junction rule requires

$$I_k(d_E) + I_{k+1}(d_S) = 0\,. \tag{13}$$

This is represented in

$$\underbrace{\begin{bmatrix} e^{-\gamma_k d_E} & -e^{\gamma_k d_E} & e^{-\gamma_{k+1} d_S} & -e^{\gamma_{k+1} d_S} \end{bmatrix}}_{=\Gamma_{CL}} \cdot \begin{bmatrix} I_{i,k} \\ I_{r,k} \\ I_{i,k+1} \\ I_{r,k+1} \end{bmatrix} = 0\,. \tag{14}$$

Using the Tikhonov regularization to solve this problem takes the junction rule in account:

$$\min_{\mathbf{I}} \left(\left\| (\mathbf{\Psi} \cdot \mathbf{D}_l \cdot \mathbf{K}_{sub} \cdot \mathbf{K}_{CL}) \cdot \mathbf{I} - \mathbf{H} \right\|_2^2 + \alpha \left\| \mathbf{\Gamma}_{CL} \cdot \mathbf{I} \right\|_2^2 \right) \tag{15}$$

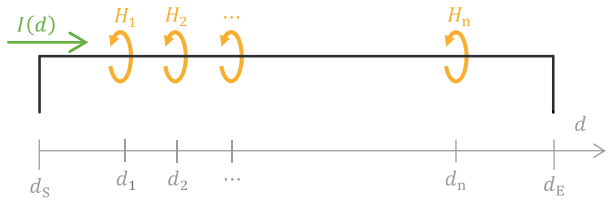

Fig. 4. Schematic presentation of the current flowing in a line and the induced magnetic field.

Evaluating the solution **I** of the inverse problem, the incident and reflected waves for every line are known. This allows the calculation of the current distribution by using (7). Besides, it is also possible to determine the termination impedance of every line or rather section that is represented in this form.

In the following, the workflow for determining the termination is shown for the example in Fig. 3 or rather (12). In addition to the current distribution, with knowledge of the wave impedance $Z_{0,k}$, the voltage distribution $V_k(d)$ along the k-th line can be calculated by

$$V(d) = Z_{0,k} \cdot \left(I_{i,k} e^{-\gamma_k d} + I_{r,k} e^{\gamma_k d} \right). \tag{16}$$

The evaluation of current and voltage at the end of the line provides the termination Z_E:

$$Z_E = \frac{V(d_E)}{I(d_E)} = Z_{0,k} \cdot \frac{I_{i,k} e^{-\gamma_k d_E} + I_{r,k} e^{\gamma_k d_E}}{I_{i,k} e^{-\gamma_k d_E} - I_{r,k} e^{\gamma_k d_E}} \tag{17}$$

B. Simplified Determination of Current Distribution and Termination

Another approach to estimate the current distribution and the line termination is a stepwise determination. This is done pragmatically with an evaluation of the magnetic field directly above the investigated lines (see Fig. 4). Considering the field in close vicinity to the line, it is dominated by the current distribution $I(d)$ of the observed line. Hence, there is the relation

$$I(d) = c \cdot H(d)\,. \tag{18}$$

The correction factor c is defined by a calibration for a constant frequency and a fixed distance to the line. This relationship only is viable for areas of the line that are far enough from the ends, as the magnetic field of an infinite long conductor with an infinitesimal cross section is assumed. Thus, the current distribution results directly from the data of the magnetic field. By using the description of (8), an inverse problem is formulated to calculate the incident and reflected wave. The least square method could be used successfully to solve this problem. Same as before, the termination results from the determined waves (see (17)).

IV. Simulation Based Investigation of Current Distribution Determination

In this section, the improved method to reconstruct current distributions is used to determine the current distribution of a complex structure with five current paths. The results are compared to the calculated distributions of the basic method without consideration of the transmission-line theory (simple multi-dipole-model in (2)). Fig. 5 shows the investigated PCB-like structure. Every line is stimulated by a Thévenin source at the near end, which is the left end of the lines shown in Fig. 5. The stimuli and the termination impedances at the other ends of the lines are listed in Table I.

The structure is simulated with the field simulation program CONCEPT-II [8]. Here, the lines are represented as round conductors with a radius of 0.07 mm at a height of 1.5 mm over the ground plane. Basic data for the reconstruction methods is the magnetic field 8 mm above the ground plane. It is simulated in an equidistant 145 mm × 100 mm grid with a spacing of 5 mm

(see Fig. 5). Varying the amplitude about ± 2 dB of the computed field data and adding a noise signal about $-50\ \mathrm{dB_{A/m}}$, the simulated field distribution is closer to measurement data.

The utilized multi-dipole-model consists of 230 dipole-triples. Every vertical section of the structure is discretized with 5 dipoles. On the horizontal sections, the lengths of the dipoles is about 3 mm. The number of dipoles for the horizontal and vertical sections of every line is listed in Table I.

In Fig. 6, the reconstructed current distributions of the lines 3, 4 and 5 for 100 MHz and 1 GHz are shown. For both frequencies, the enhanced method considering the transmission-line theory widely improves the precision of the reconstruction. Even for currents differing by up to 25 dB the method produces accurate results. The biggest relative deviation occurs for the reconstructed amplitude on line 4 for 1 GHz. Here, the deviation is negligible because of the low current strength. In addition, the analysis of the reconstructed phase shows a high conformity to the simulated distribution. Thus, the wave phenomena are correctly identified and represented due to the transmission-line theory.

V. Simulation Based Investigation of Termination Determination

At this point, the approaches for determining the termination impedance of chapter III are discussed by applying the methods on simulation data of PCB-like structures. In CONCEPT II, the magnetic near field-data for two different examples is calculated. Below, these methods are referred to as either "direct reconstruction" (chapter III. A) or "successive" (chapter III. B).

A. Determination of a Termination Impedance at a Single Line

Initially, for a single line above ground the method to determine the terminations is exemplarily investigated. The line has a length of 10 cm, a height of 1.5 mm over ground plane and a radius of 0.1 mm. Losses are neglected. At the near end on the vertical element, a Thévenin source (1 V, 50 Ω) stimulates the setup. The termination impedance of the vertical element at the far end of the line is varied. Its estimation is investigated in a frequency range from 1 MHz to 3 GHz.

The initial data for both approaches is the magnetic field exactly above the line at heights h of 2 mm, 4 mm and 6 mm. It is calculated at several points, distance between points is related to the wavelength λ. All points are distributed with a distance of approximately $\lambda/60$, but for low frequencies there are at least 10 points.

In the investigation with the multi-dipole-model, each vertical section is represented with 5 dipoles and the horizontal section with 200 dipoles (0.5 mm spacing of dipoles). This fine discretization is necessary because of the shortest chosen observation height of 2 mm. For an acceptable field approximation, the spacing of the dipoles must be equal or smaller than the observation distance, due to the point source characteristics of the dipole.

To investigate both methods, the estimated termination impedance is compared to the actual value used in the simulation model. This is the known termination in addition to a serial in-

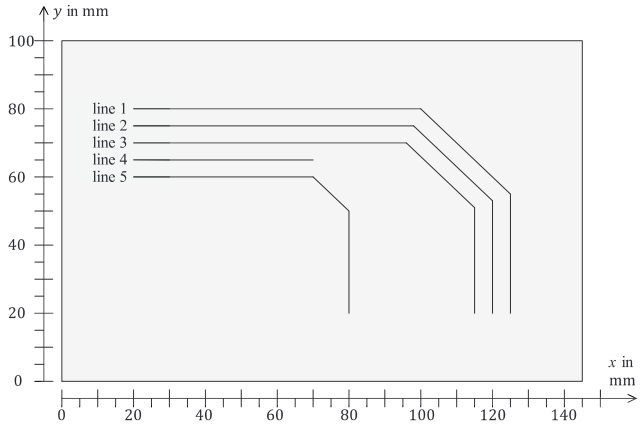

Fig. 5. Examplary challenging PCB-like structure.

TABLE I
Circuits at Far End and Near End of Lines in Examplary PCB-Like Structure

line number	stimulus (near end)	termination (far end)	number of dipoles
1	$5\ \mathrm{V}\ e^{j240°}, 50\ \Omega$	50 Ω	55
2	$5\ \mathrm{V}\ e^{j120°}, 50\ \Omega$	50 Ω	55
3	$5\ \mathrm{V}\ e^{j0°}, 50\ \Omega$	50 Ω	55
4	$2\ \mathrm{V}\ e^{j180°}, 50\ \Omega$	1 mΩ	25
5	$3\ \mathrm{V}\ e^{j0°}, 50\ \Omega$	1 kΩ	40

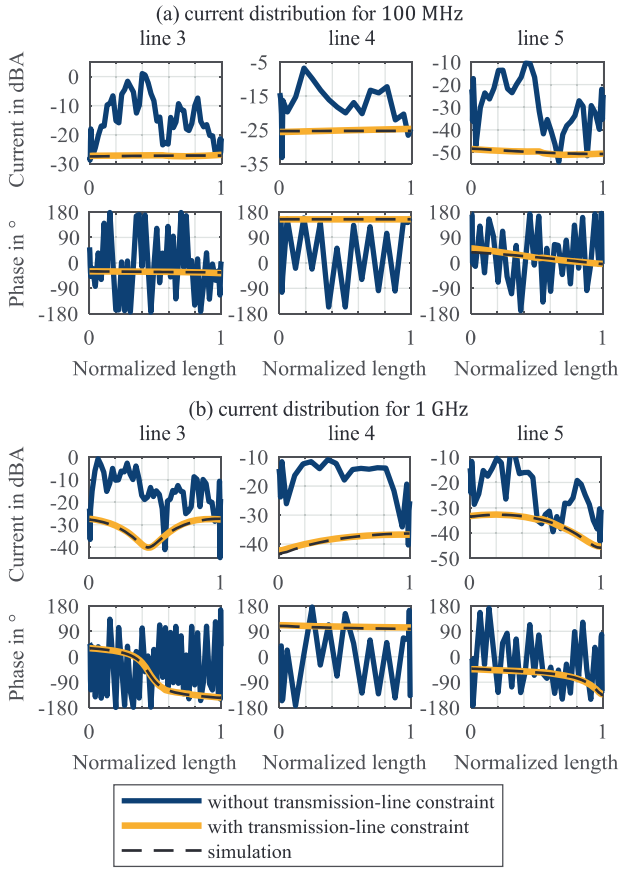

Fig. 6. Reconstructed current distributions using the enhanced method compared with simulation data (reference) and the basic method.

ductor and a parallel capacitor. Both elements describe the parasitic effects of the vertical section. They are estimated with 700 pH and 20 fF. Disregarding parasitic effects, the real part of the estimated termination impedance $Z_{\mathrm{T,esti}}$ is investigated. Fig. 7 shows this comparison for the different terminations (50 Ω, 200 Ω and 500 Ω). The wire has a wave impedance of 204 Ω, i.e. these terminations represent important reflection factors ($r < 0, r \approx 0, r > 0$).

The investigation shows that the simple method with a successive reconstruction gives accurate impedance values for very small measurement heights. The method of direct reconstruction is more suitable for estimating the line termination in greater heights.

B. *Determination of a Termination Impedance at a Parallel Lines Setup*

After proving the feasibility for a simple example, the methods are used to investigate a configuration of two parallel lines. The setup is made of two instances of the line from the section before. Both lines are stimulated by identical Thévenin sources (1 V, 50 Ω), but terminated differently. Line 1 is terminated with $R_{\mathrm{T1}} = 50\ \Omega$. To impede the reconstruction, the second line has a termination close to the wave impedance ($R_{\mathrm{T2}} = 200\ \Omega$). Thus, there is a mostly homogenous current distribution making the reconstruction of the values on line 1 more complicated because of an interfering field.

To investigate the results of both reconstruction methods, the distance d between the lines is varied by 1 cm, 2 cm and 3 cm. As before, the magnetic field is calculated at the heights 2 mm, 4 mm and 6 mm above the ground plane. Also, the lines are represented with the same multi-dipole-model as before.

The estimated impedance $Z_{\mathrm{T1,esti}}$ of the termination R_{T1} is shown in Fig. 8. As before, taking parasitic effects into account, inductive and capacitive effects at the end of the lines are considered and the real part of the estimated impedance is examined.

Using the successive reconstruction, the estimated termination value shows less precise results than in the investigation before. Generally, for greater distances between the lines, the coupled field decreases. Therefore, the estimation is not as much affected by the field of the second line. This is shown by the reconstructed value for all investigated cases. Overall, the termination is better estimated with a direct reconstruction. This is primary based on the process to identify the current distribution on all lines in one inverse problem considering all currents as field sources.

VI. Determination of Terminations from Measured Magnetic Field Data

Finally, the direct reconstruction method for determining termination impedances is applied to a real setup. The setup is shown in Fig. 9 and can be seen as a simple PCB representation. The radius of all lines is 0.39 mm and the distance between the lines is 7.5 mm. They have a height of 1.95 mm. For the wire system, vacuum propagation characteristics are assumed. All lines are terminated with 50 Ω resistors (right side on the figure) and stimulated with a function generator (50 MHz square wave with 1 V_{pp} amplitude via power splitter, left side on the figure).

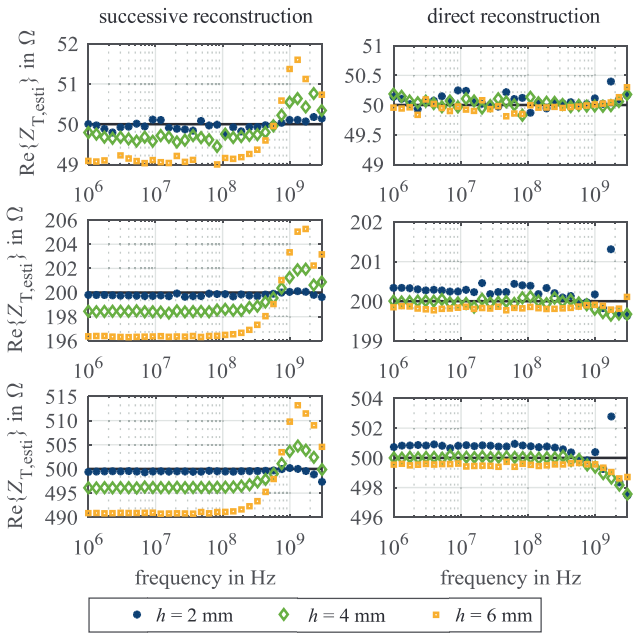

Fig. 7. Comparison of the estimated impedance $Z_{\mathrm{T,esti}}$ for several termination impedances of a single line for different observation heights h of the magnetic field.

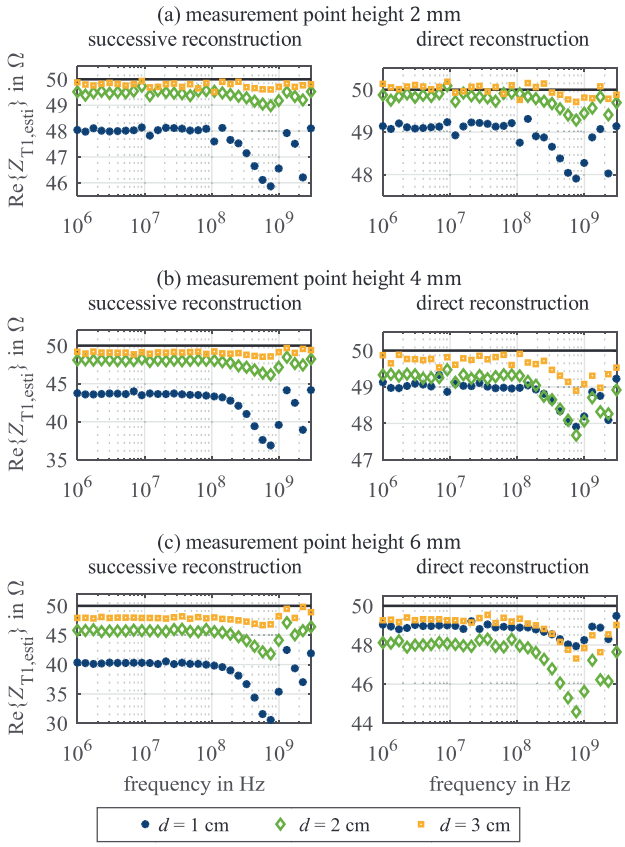

Fig. 8. Comparision of the estimated termination impedance $Z_{\mathrm{T1,esti}}$ in the parallel line configuartion for several line distances.

For several heights, the field is measured exactly above the line. The measurement points are gridded with 1 mm distance. The points in a distance of less than 1 cm to the near or far end of the lines are not considered. Thus, there are no measurement points above line 1 and 3 close to the far end of line 2 (see Fig. 9). Only the field component orthogonal to the lines is measured.

To measure the magnetic field with amplitude and phase, a probe (Langer EMV MFA-R 0.2-75) and an oscilloscope (Teledyne LeCroy WavePro 760Zi-A) are used. By applying an FFT, the measured data is transformed into the frequency domain and, therefore, known in magnitude and phase.

For the reconstruction, a multi-dipole-model made of 168 dipoles is used (3 dipoles at vertical sections, 30 dipoles per 5 cm at horizontal sections). In the inverse problem, the setup is modeled by two (multi-transmission-) line systems: three and two parallel lines. They are described as section 1 and section 2 in Fig. 9. Using this model, the superposition of the incident and reflected waves on the different areas on the lines is considered.

The calculated termination impedances $Z_{\mathrm{T1,esti}}$, $Z_{\mathrm{T2,esti}}$ and $Z_{\mathrm{T3,esti}}$ for line 1, 2 and 3 are shown in Fig. 10. Here, the real and imaginary part of the impedances are independently presented. Thus, the real part can be compared to the installed termination. Parasitic effects of the used terminations, connection cables, and connectors have a major impact on the imaginary part.

It can be found that the terminations are close to the expected values for high frequencies. In particular, for the nearest measurement, the estimated impedance agrees well with the actual values for the lines 1 and 3. Noise from the measurement setup, numerical errors from the signal processing, and the weak decoupling between near and far end might be reasons for deviations.

VII. Conclusion and Outlook

In this work, a reconstruction method for current distributions by magnetic near-field data was extended by applying the transmission-line theory as an additional constraint. In the shown examples, this feature widely improved the quality of the calculated current distributions. Furthermore, the approach enabled the calculation of the incident and reflected wave of the lines in the investigated structure. From these insights, a method has been developed to determine the termination impedances of the lines. A good agreement between simulation and measurement has been found. Especially for high frequencies, the presented methods were able to estimate the terminations in the investigated structures. For low frequencies, the estimated termination values were less accurate. Here, further investigations are required. One possible approach is the usage of frequency domain measurement technology. In this case, the presented methods must be adjusted to enable the calculation based on only magnitude fields. Further works will apply multiconductor transmission-line theory for better estimation of the termination impedances.

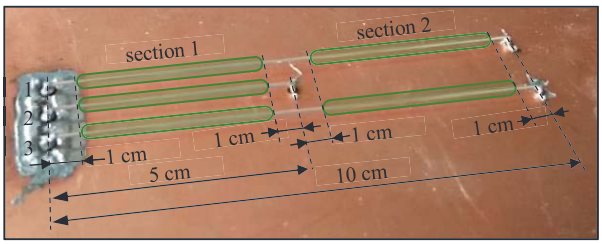

Fig. 9. Measurement setup for investigation of terminations. Areas for observation points are marked green.

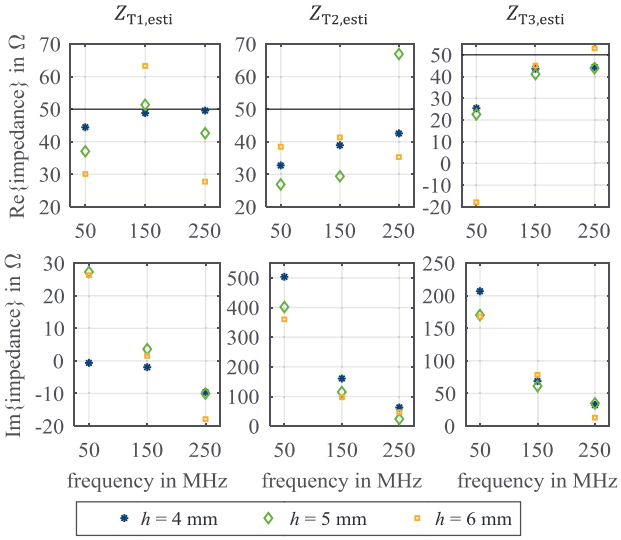

Fig. 10. Determined termination of the measurement setup for different frequencies and measurement heights.

References

[1] X. Gao, J. Fan, Y. Zhang, H. Kajbaf and D. Pommerenke, "Far-Field Prediction Using Only Magnetic Near-Field Scanning for EMI Test," *IEEE Trans. Electromagn. Compat.*, vol. 56, no. 6, pp. 1335 – 1343, May 2014.

[2] H. Shall, K. Alameh, Z. Riah, A. Alaeddine and M. Kadi, "A tridimensional radiated emission model based on an improved near field scan technique," in *2014 International Conference on Green Energy*, Sfax, 2014, pp. 240 – 245.

[3] D. Rinas, P. Ahl and S. Frei, "PCB current identification based on near-field meas-urements using preconditioning and regularization," *Adv. Radio Sci.*, vol. 14, pp. 121 – 127, Sept. 2016.

[4] C. R. Paul, *Introduction to electromagnetic compatibility*, 2nd ed. Hoboken, NJ, USA: Wiley, 2006.

[5] X. Tong, D. W. P. Thomas, A. Nothofer, P. Sewell and C. Christopoulos, "Modeling Electromagnetic Emissions From Printed Circuit Boards in Closed Environments Using Equivalent Dipoles," *IEEE Trans. Electromagn. Compat.*, vol. 52, no. 2, pp. 462 – 470, May 2010.

[6] Z. Yu, J. A. Mix, S. Sajuyigbe, K. P. Slattery and J. Fan, "An Improved Dipole-Moment Model Based on Near-Field Scanning for Characterizing Near-Field Coupling and Far-Field Radiation From an IC," *IEEE Trans. Electromagn. Compat.*, vol. 55, no. 1, pp. 97 – 108, Feb. 2013.

[7] D. Rinas, S. Niedzwiedz, J. Jia and S. Frei, "Optimization Methods for Equivalent Source Identification and Electromagnetic Model Creation based on Near-Field Measurements," in *EMC Europe 2011*, York, 2011, pp. 298 – 303.

[8] Institute of Electromagnetic Theory, Hamburg University of Technology (TUHH), Germany. *CONCEPT-II*. (2018) [Online]. Available: http://www.tet.tuhh.de/concept/?lang=en.